

Article

Effect of Crack Initiation and Life Prediction of Polyacrylonitrile-Reinforced Gussasphalt Surfacing over Steel Bridge Deck under Fiber Content Variation

Xun Qian Xu, Wei Yang, Hong Liang Xiang *, Jian Bo Wang and Xiao Yang

National & Local Joint Engineering Research Center of Technical Fiber Composites for Safety and Health, Nantong University, Nantong 226019, China; xunqian_xu@ntu.edu.cn (X.Q.X.); weiyang_ntu@163.com (W.Y.); jianbo_wang@163.com (J.B.W.); yangxiao_ntu@163.com (X.Y.)

* Correspondence: hongliang_xiang@163.com; Tel.: +86-135-1521-2080

Received: 14 January 2020; Accepted: 24 February 2020; Published: 28 February 2020



Abstract: The crack initiation and life prediction of fiber-reinforced asphalt concrete (FRAC) surfacing for steel bridge decks under a cyclic vehicle load are analyzed from the perspective of damage mechanics. The damage field and the stress and strain field evolution rule of a composite beam in fatigue test are studied, and a fatigue failure criterion is proposed for steel deck FRAC surfacing. Bending fatigue tests are performed on composite beams composed of a steel deck and polyacrylonitrile (PAN)-fiber-reinforced Gussasphalt (GA), i.e., GA-PAN, concrete surfacing under different fiber content and temperature conditions. The damage evolution characteristics of GA-PAN concrete surfacing over the steel deck with different fiber lengths and volume ratios are predicted by analyzing the fatigue life equations. The results show that the steel bridge deck FRAC surfacing model can reflect the comprehensive influence of the fiber content and length on the fatigue performance of steel bridge AC. Specifically, a lower temperature results in the fiber more synergistically affecting the fatigue resistance of AC. Theoretically, the service performance of asphalt concrete increases with the increase of fiber length and content. The optimum fiber length and volume ratio of GA-PAN are found to be 9 mm and 0.46–0.48%, respectively, considering the construction workability.

Keywords: steel bridge deck surfacing; Gussasphalt; fatigue damage; fatigue life evaluation; polyacrylonitrile

1. Introduction

The Gussasphalt (GA) mixture with high viscosity was first applied in Germany (1982), and since then, it was widely used in Britain, Japan, and China. In the late 1990s, the Jiangyin Yangtze River Highway Bridge in China introduced the British single-layer pouring surfacing structure. This surfacing project was under the general contract of the Klohn Crippen Berger (KCB) engineering company in the United Kingdom (UK). Compared with the ordinary asphalt mixture, GA has better high-temperature resistance and lesser low-temperature crack resistance [1,2]. After the bridge was completed and opened to traffic, several longitudinal cracks began to appear within several months [3–5]. Asphalt concrete (AC) surfacing is an important part of the steel bridge deck, and the cracking of asphalt surfacing in the bridge deck not only degrades the mechanical properties of the asphalt but also causes the secondary deterioration of the steel bridge deck, greatly reducing the service life of the bridge [6,7]. Fatigue damage and the cracking of the asphalt surfacing are major problems restricting the use efficiency of bridges. Thus, improving the fatigue damage resistance of asphalt surfacing steel bridge decks has both theoretical and engineering significance [8,9]. Compared with ordinary AC, fiber-reinforced asphalt concrete (FRAC) has the advantages of a higher strength and modulus, good

creep resistance, aging resistance, impact toughness, and designability [10]. FRAC is widely used in high-speed road networks, urban trunk roads, and national trunk lines, especially for special asphalt surfacing steel bridge deck surfacing [11–13].

Because asphalt mixtures are rich in microscale defects, microcracks appear in the asphalt after loading and gradually expand under the periodic action of the load, eventually damaging the asphalt material [14–16]. Traditionally, fatigue cracks in asphalt surfacing are defined as cracks that occur when the bending tensile stress at the bottom of the asphalt structural layer or in the semi-rigid base layer exceeds the fatigue strength of the material under the repeated action of driving loads [17]. Steel bridge deck asphalt surfacing is a special type of surfacing material with a typical orthotropic structure. Its mechanical and service properties change significantly with structural changes. Therefore, the generation mechanism and development process underlying the fatigue cracking of a steel bridge deck asphalt structure are not only affected by repeated driving loads but are also closely related to the stress distribution of the bridge deck structure [18–20].

The fatigue performance of FRAC was researched mainly using phenomenological, mechanical approximation, and damage mechanics methods [21–23]. Meanwhile, over the past few decades, the fatigue performance of AC was studied using different test methods, such as full-scale testing, beam bending, and splitting [24–26]. Furthermore, viscoelastic, damage mechanics, and energy dissipation models were established to describe the fatigue performance of AC [27,28]. The influence of the stress level, frequency, temperature, and loading mode on the fatigue performance of steel bridge deck AC was also discussed [29–31]. However, the fatigue model is the core of AC surfacing fatigue performance research [32]. The existing methods for predicting the fatigue life of AC include fatigue models related to only strain, both strain and stiffness, or strain, stiffness, and volume parameters [33,34]. Based on fatigue tests, researchers analyzed the factors that affect the fatigue performance of asphalt mixtures and their influence laws and proposed a variety of fatigue life prediction models for asphalt mixtures. Many of these models were adopted as asphalt surfacing structural design methods in different countries and institutions [35–37].

At present, the influence of the fiber type, length, and content ratio on the fatigue performance of AC is mainly studied based on the fatigue test under the stress and strain control modes [38,39]. However, reviewing the existing research reveals that some problems remain, such as the influence of fatigue test methods and fatigue failure criteria on the fatigue life of FRAC and the unification of fatigue failure criteria of FRAC. Furthermore, the comprehensive influence of the fiber content and length on the fatigue performance of steel deck AC remains unknown, as does the mechanism underlying the effect of PAN fiber on the fatigue performance of steel deck AC.

In this study, the ratios of the average fiber length (L_f) and fiber volume to asphalt mixture volume (V_f) are taken as variables. Bending fatigue tests are performed on a composite beam with polyacrylonitrile-fiber-reinforced Gussasphalt (GA-PAN) on a steel bridge deck under stress control mode, and the damage evolution rule of steel deck FRAC surfacing is analyzed using the results. Based on the theory of damage mechanics, a fatigue failure criterion for FRAC surfacing is proposed, which combines the phenomenological and damage mechanics methods. The influence of V_f and L_f of PAN on the fatigue damage of steel deck GA concrete is analyzed systematically, and a model for calculating the fatigue life of steel deck FRAC surfacing is established, which considers the influence of characteristic parameters of fiber length and content.

2. Experimental Model and Damage Evolution Theory for Fatigue Analysis

2.1. Experimental Model Design of Steel Deck FRAC Surfacing

In applications of steel bridge deck AC surfacing engineering, longitudinal cracks were observed on the asphalt surface above the u-stiffener of the steel box girder owing to the repetitive action of the vehicle load [40]. According to the environmental conditions of steel deck applications, the FRAC surfacing on steel decks is simplified as a composite beam structure. In order to facilitate this

research, a double-layer composite beam model composed of the steel bridge deck FRAC surfacing was established, taking Jiangyin Yangtze River long-span steel deck surfacing structure as an example [6]. The results of a finite element analysis (Figure 1a, ANSYS14.0, Pittsburgh, PA, USA) show that the control stress/strain of the surfacing is the maximum transverse tensile stress/strain, which is located on the surfacing surface above the trapezoidal stiffener (Figure 1b). Because of the orthotropic characteristics of the steel box girder deck, the trapezoid stiffener under it has an obvious local effect on the consolidation support of the deck (at point A), which is an area sensitive to fatigue cracking.

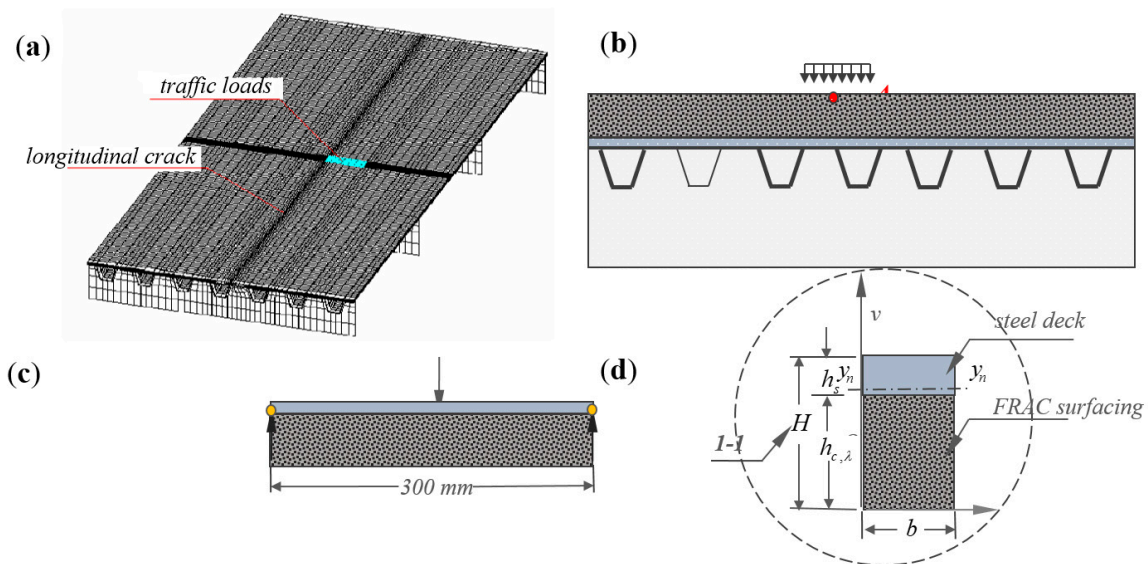


Figure 1. Steel deck fiber-reinforced asphalt concrete (FRAC) surfacing composite beam for fatigue analysis: (a) orthotropic local finite element model; (b) critical position of the vehicle wheel load; (c) composite beam equipment for fatigue testing; (d) cross-section of the double-layer composite beam.

In order to study the fatigue characteristics of AC surfacing on the steel bridge deck, a composite beam specimen matching the actual load conditions was designed for relevant experiments. When the automobile load acts on the steel plate (the upper surface of the sample), fatigue cracking appears in the midspan of the composite beam for the steel deck AC surfacing (Figure 1c). A cross-section of the double-layer composite beam is shown in Figure 1d. In the subsequent fatigue analysis, h_s is the thickness of steel deck (mm), $h_{c,\lambda}$ is the thickness of the FRAC surfacing (mm), H is the total thickness of the double-layer composite beam (mm), i.e., $H = h_s + h_{c,\lambda}$, y is the vertical distance from any point to the edge of the beam bottom (mm), y_n is vertical distance between the neutral axis and the bottom edge of the beam, and b is the width of the composite beam (mm).

2.2. Damage Evolution Equations of Composite Beam for the Steel Deck FRAC Surfacing

Generally, the fatigue test data can be obtained from the loading stress, cycle times, deflection, and deformation of composite beams, but the damage information of the specimen is not easily measured or deduced. Therefore, Zhang et al. proposed the following fatigue damage evolution equation based on experimental test information [41]:

$$dD/dN = a^* \cdot [\sigma / (1 - D)]^p \cdot (1 - D)^{-q}, \quad (1)$$

where p , q , and a^* are material parameters related to test conditions including loading level and environment temperature, σ is the stress at a point on the control section of the beam, and D is the damage variable. According to the theory of damage mechanics, D is equal to 0 when the specimen is in its original undamaged state, and D is equal to 1 when the specimen forms cracks.

Using the concept of effective stress, the following elastic damage constitutive equation can be obtained:

$$\sigma = E(1 - D)\varepsilon, \quad (2)$$

where ε is the strain at a point on the control section of beam, and E is the elastic modulus of the test material. Substituting Equation (2) into Equation (1) and using equivalence condition $a = a^*E^p$,

$$dD/dN = a \varepsilon^p (1 - D)^{-q}. \quad (3)$$

Based on the strain equivalent principle, the equivalent stress at any point of the test beam as shown in Figure 1d is calculated as follows:

$$\bar{\sigma}(\xi) = \sigma(\xi) / [1 - D(\xi)] = E_{c,\lambda} \cdot \varepsilon(\xi), \quad (4)$$

where $\xi = y/H$, $\bar{\sigma}(\xi)$, $\sigma(\xi)$, $\varepsilon(\xi)$, and $D(\xi)$ are the equivalent stress, stress, strain, and degree of damage at any position ξ , respectively, and $E_{c,\lambda}$ denotes the elastic modulus of the FRAC surfacing, $E_{c,\lambda} = f(L_f, V_f)$.

Under a cyclic load, the steel deck FRAC surfacing composite beam mainly cracks in the surfacing. The static balance requirements of the middle span cross-section of the test beam are as follows:

$$\int_0^{\frac{h_{c,\lambda}}{H}} bHE_{c,\lambda}[1 - D(\xi)]\varepsilon(\xi) d\xi + \int_{\frac{h_{c,\lambda}}{H}}^1 bHE_s\varepsilon(\xi) d\xi = 0, \quad (5)$$

$$\int_0^{\frac{h_{c,\lambda}}{H}} bH^2E_{c,\lambda}[1 - D(\xi)]\varepsilon(\xi) \xi d\xi + \int_{\frac{h_{c,\lambda}}{H}}^1 bH^2E_s\varepsilon(\xi) \xi d\xi = M, \quad (6)$$

where E_s and M are the elastic modulus of the steel bridge deck and the bending moment of the composite beam at the middle of the span, respectively.

According to the damage mechanics theory of continuous medium, it is presumed that $\xi_n = y_n/H$, $\rho = \frac{\xi_n - \xi}{\xi_n}$, and $q = 0$.

Substituting Equation (4) into Equation (6) gives

$$d\xi = -\xi_n d\rho, \quad (7)$$

$$\varepsilon(\xi) = \varepsilon_{cm}(N) \left(\frac{\xi_n - \xi}{\xi_n} \right) = \varepsilon_{cm}(N) \cdot \rho, \quad (8)$$

where $\varepsilon_{cm}(N)$ is the bottom edge strain of the middle span of the composite beam after N fatigue load cycles.

3. Crack Initiation and Life Prediction

3.1. Evolution of Fatigue Damage Degree for the Steel Deck FRAC Surfacing

Substituting Equations (7) and (8) into Equation (5) and solving gives

$$\int_1^{1 - \frac{h_{c,\lambda}}{H\xi_n}} E_{c,\lambda} \cdot [1 - D(\rho)] \cdot \rho d\rho + \int_{1 - \frac{h_{c,\lambda}}{H\xi_n}}^{1 - \frac{1}{\xi_n}} E_s \cdot \rho \cdot d\rho = 0. \quad (9)$$

By solving Equation (9), the following equation can be obtained:

$$\int_{1 - \frac{h_{c,\lambda}}{H\xi_n}}^1 \rho \left(\int_0^N D(\rho) dN \right) d\rho = (E_s/E_{c,\lambda} + h_{c,\lambda}/H - E_s h_{c,\lambda}/E_{c,\lambda} H) / \xi_n + (E_s \cdot h_{c,\lambda}^2/E_{c,\lambda} H^2 - h_{c,\lambda}^2/H^2 - E_s/E_{c,\lambda}) / 2\xi_n^2 \quad (10)$$

Solving Equation (9) and integrating Equation (10), the solution of $\int_{1-\frac{h_{c,\lambda}}{H\xi_n}}^1 \rho \left(\int_0^N D(\rho) dN \right) d\rho$ can be obtained as follows:

$$\int_{1-\frac{h_{c,\lambda}}{H\xi_n}}^1 \rho \left(\int_0^N D(\rho) dN \right) d\rho = \left[1 - \left(1 - \frac{h_{c,\lambda}}{H\xi_n} \right)^{p+2} \right] \cdot \frac{D_{cm}(N)}{p+2}. \tag{11}$$

Combining Equation (10) and Equation (12), the solution of $D_{cm}(N)$ is deduced as follows:

$$D_{cm}(N) = (p+2) \cdot \left[1 - \left(1 - \frac{h_{c,\lambda}}{H\xi_n} \right)^{p+2} \right] \cdot \left[\frac{1}{\xi_n} \left(\frac{E_s}{E_{c,\lambda}} + \frac{h_{c,\lambda}}{H} - \frac{E_s}{E_{c,\lambda}} \cdot \frac{h_{c,\lambda}}{H} \right) + \frac{1}{2\xi_n^2} \left(\frac{E_s h_{c,\lambda}^2}{E_{c,\lambda} H^2} - \frac{h_{c,\lambda}^2}{H^2} - \frac{E_s}{E_{c,\lambda}} \right) \right], \tag{12}$$

where $D_{cm}(N)$ is the damage degree at the bottom edge of the middle span on the composite beam after N fatigue load cycles. When fatigue cracking initiation, $D_{cm}(N)$, is equal to 1.0, the corresponding N_{cr} is the fatigue life of the steel deck FRAC surfacing.

3.2. Evolution of the Stress and Strain Distributions for the Steel Deck FRAC Surfacing

By solving Equation (6), the following equation is obtained:

$$\int_{1-\frac{h_{c,\lambda}}{H\xi_n}}^1 D(\rho) \cdot (\rho - \rho^2) d\rho - \int_{1-\frac{h_{c,\lambda}}{H\xi_n}}^1 (\rho - \rho^2) d\rho + \frac{E_s}{E_{c,\lambda}} \int_{1-\frac{h_{c,\lambda}}{H\xi_n}}^{1-\frac{1}{\xi_n}} (\rho - \rho^2) d\rho = \frac{-M}{E_{c,\lambda} \cdot b H^2 \varepsilon_{cm}(N) \xi_n^2}. \tag{13}$$

The first term on the left side of Equation (13) is

$$A = \int_{1-\frac{h_{c,\lambda}}{H\xi_n}}^1 D(\rho) \cdot (\rho - \rho^2) d\rho = \int_{1-\frac{h_{c,\lambda}}{H\xi_n}}^1 (\rho - \rho^2) \left[\int_0^N \left(\frac{dD}{dN} \right) dN \right] d\rho = D_{cm}(N) \cdot \left[\left(1 - \left(1 - \frac{h_{c,\lambda}}{H\xi_n} \right)^{p+2} \right) / (p+2) - \left(1 - \left(1 - \frac{h_{c,\lambda}}{H\xi_n} \right)^{p+3} \right) / (p+3) \right] \tag{14}$$

The second term on the left side of Equation (13) is

$$B = - \int_{1-\frac{h_{c,\lambda}}{H\xi_n}}^1 (\rho - \rho^2) d\rho = \left(3 \left(1 - \frac{h_{c,\lambda}}{H\xi_n} \right)^2 - 2 \left(1 - \frac{h_{c,\lambda}}{H\xi_n} \right)^3 - 1 \right) / 6. \tag{15}$$

The third term on the left side of Equation (13) is

$$C = \frac{E_s}{E_{c,\lambda}} \int_{1-\frac{h_{c,\lambda}}{H\xi_n}}^{1-\frac{1}{\xi_n}} (\rho - \rho^2) d\rho = \frac{E_s}{E_{c,\lambda}} \cdot \left[\left(\left(1 - \frac{1}{\xi_n} \right)^2 - \left(1 - \frac{h_{c,\lambda}}{H\xi_n} \right)^2 \right) / 2 - \left(\left(1 - \frac{1}{\xi_n} \right)^3 - \left(1 - \frac{h_{c,\lambda}}{H\xi_n} \right)^3 \right) / 3 \right] \tag{16}$$

The middle-span bending moment can be expressed as

$$M = -E_{c,\lambda} \cdot b \cdot H_0^2 \cdot \varepsilon_{cm}(0) / 6, \tag{17}$$

where H_0 is the equivalent height and can be obtained as follows:

$$H_0 = \frac{E_{c,\lambda} H^3}{12(1 - \nu_{c,\lambda}^2)} = \sqrt[3]{h_{c,\lambda}^3 + \frac{E_s h_s^3 (1 - \nu_{c,\lambda}^2)}{E_{c,\lambda} (1 - \nu_s^2)} + \frac{3E_s h_{c,\lambda} h_s H^2}{(1 - \nu_s^2)(E_{c,\lambda} h_{c,\lambda} + E_s h_s)} \kappa}, \tag{18}$$

where $\nu^{c,\lambda}$ and ν_s are Poisson's ratios of the FRAC surfacing and steel bridge deck, respectively, and κ is the bonding coefficient between the steel deck and the FRAC concrete. In addition, $\kappa = 0$ denotes that the slippage damage is caused by the complete debonding of FRAC surface from the steel bridge deck, while $\kappa = 1$ means that the FRAC surface perfectly bonds with the steel deck.

Combining Equations (13) and (17), the bottom edge strain of middle span on the composite beam after N fatigue load cycles can be deduced to be

$$\varepsilon_{cm}(N) = H_0^2 \varepsilon_{cm}(0) / 6H^2 \xi_n^2 (A + B + C). \quad (19)$$

By substituting Equation (19) into Equation (7), the strain and stress of any position on middle span cross-section can be derived as

$$\varepsilon(\xi) = \varepsilon_{cm}(N) \cdot \rho = H_0^2 \varepsilon_{cm}(0) \rho / 6H^2 \xi_n^2 (A + B + C), \quad (20)$$

$$\sigma(\xi) = \varepsilon_{cm}(N) \cdot \rho = E_{c,\lambda} [1 - D(\xi)] H_0^2 \varepsilon_{cm}(0) \rho / 6H^2 \xi_n^2 (A + B + C). \quad (21)$$

3.3. Fatigue Life Prediction for the Steel Deck FRAC Surfacing

The degree of damage and the distribution of the steel deck FRAC surfacing can be described by Equations (11)–(13) after N fatigue load cycles. $D_{cm}(N) = 1$ indicates that crack initiation and fatigue failure can be detected on the composite structure. Substituting Equation (19) into Equation (2) gives

$$\frac{dD(N)}{dN} = a \varepsilon_m^p(N) = a \cdot \left(\frac{H_0^2 \varepsilon_m(0)}{6H^2 \xi_n^2 (A + B + C)} \right)^p. \quad (22)$$

By differentiating Equation (12) and substituting into Equation (22), the following equation can be derived:

$$\begin{aligned} & a \cdot \varepsilon_{cm}^p(0) d(N) \\ &= (A + B + C)^p d\xi_n \cdot (p + 2) \cdot (6H^2 \xi_n^2)^p / \{H_0^{2p} \cdot [1 - (1 - h_{c,\lambda}/H\xi_n)^{p+2}]\}. \\ & \left[\left(\frac{E_s}{E_{c,\lambda}} + \frac{h_{c,\lambda}}{H} - \frac{E_s}{E_{c,\lambda}} \cdot \frac{h_{c,\lambda}}{H} \right) / \xi_n + \left(\frac{E_s \cdot h_{c,\lambda}^2}{E_{c,\lambda} H^2} - \frac{h_{c,\lambda}^2}{H^2} - \frac{E_s}{E_{c,\lambda}} \right) / 2\xi_n^2 \right] \end{aligned} \quad (23)$$

By integrating both sides of Equation (23), the equation is deduced as

$$a \cdot \varepsilon_m^p(0) N_f = \int_{\xi_0}^{\xi_N} D \cdot (A + B + C)^p d\xi_n, \quad (24)$$

where ξ_0 is the initial neutral axis position. When $N = 0$, Equation (24) can be expressed as

$$a \cdot \varepsilon_{cm}^p(0) = D_0 \cdot (A_0 + B_0 + C_0)^p \cdot (d\xi_n/dN), \quad (25)$$

where A_0 , B_0 , C_0 , and D_0 are the initial values of A , B , C , and D , respectively.

Differentiating Equation (19) gives

$$\frac{d\xi_n}{dN} = \frac{6H^2 \xi_n^4 (A + B + C)^2}{-H_0^2 \varepsilon_{cm}(0) \cdot [2\xi_n \cdot (A + B + C) + \xi_n^2 \cdot (A' + B' + C')]} \cdot \frac{d\varepsilon_{cm}(N)}{dN}, \quad (26)$$

where parameters A' , B' , and C' can be expressed as

$$\begin{aligned}
 A' &= (p + 2) / \left[1 - (1 - h_{c,\lambda} / H\xi_n)^{p+2} \right]^2 \\
 &\cdot \left\{ \left[\left(\frac{E_s}{E_{c,\lambda}} + \frac{h_{c,\lambda}}{H} - \frac{E_s}{E_{c,\lambda}} \cdot \frac{h_{c,\lambda}}{H} \right) / \xi_n + \left(\frac{E_s \cdot h_{c,\lambda}^2}{E_{c,\lambda} H^2} - \frac{h_{c,\lambda}^2}{H^2} - \frac{E_s}{E_{c,\lambda}} \right) / 2\xi_n^2 \right] \right. \\
 &\cdot \left[(1 - (1 - h_{c,\lambda} / H\xi_n)^{p+3}) / (p + 3) - (1 - (1 - h_{c,\lambda} / H\xi_n)^{p+2}) / (p + 2) \right] \\
 &\cdot \left[(p + 2) \cdot h_{c,\lambda} \cdot (H\xi_n - h_{c,\lambda})^{p+1} / (H^{p+2} \xi_n^{p+3}) \right] - \left[1 - (1 - h_{c,\lambda} / H\xi_n)^{p+2} \right] \\
 &\cdot \left\{ \left[- \left(\frac{E_s}{E_{c,\lambda}} + \frac{h_c}{H} - \frac{E_s}{E_{c,\lambda}} \cdot \frac{h_c}{H} \right) / \xi_n^2 - \left(\frac{E_s \cdot h_c^2}{E_{c,\lambda} H^2} - \frac{h_{c,\lambda}^2}{H^2} - \frac{E_s}{E_{c,\lambda}} \right) / 4\xi_n^3 \right] \right. \\
 &\cdot \left[(1 - (1 - h_{c,\lambda} / H\xi_n)^{p+2}) / (p + 2) - (1 - (1 - h_{c,\lambda} / H\xi_n)^{p+3}) / (p + 3) \right] \\
 &- \left[\left(\frac{E_s}{E_{c,\lambda}} + \frac{h_c}{H} - \frac{E_s}{E_{c,\lambda}} \cdot \frac{h_c}{H} \right) / \xi_n + \left(\frac{E_s \cdot h_c^2}{E_{c,\lambda} H^2} - \frac{h_c^2}{H^2} - \frac{E_s}{E_{c,\lambda}} \right) / 2\xi_n^2 \right] \\
 &\cdot \left. \left[\left(1 - \frac{h_c}{H\xi_n} \right)^{p+2} - \left(1 - \frac{h_c}{H\xi_n} \right)^{p+1} \right] \left(\frac{h_c}{H\xi_n^2} \right) \right\} \\
 B' &= \left(\frac{h_{c,\lambda}}{H\xi_n^2} \right) \cdot \left(\frac{h_{c,\lambda}}{H\xi_n} - \frac{h_{c,\lambda}^2}{H^2 \xi_n^2} \right) \\
 C' &= \frac{E_s}{E_{c,\lambda} \cdot \xi_n^2} \cdot \left[\left(\frac{1}{\xi_n} - \frac{1}{\xi_n^2} \right) + \left(\frac{h_{c,\lambda}^3}{H^3 \xi_n^2} - \frac{h_{c,\lambda}^2}{H^2 \xi_n} \right) \right].
 \end{aligned}$$

When $N = 0$, Equation (26) can be expressed as

$$\left(\frac{d\xi_n}{dN} \right)_0 = \frac{6H^2 \xi_0^4 (A_0 + B_0 + C_0)^2}{-H_0^2 \varepsilon_{cm}(0) \cdot [2\xi_n \cdot (A_0 + B_0 + C_0) + \xi_n^2 \cdot (A'_0 + B'_0 + C'_0)]} \cdot \left(\frac{d\varepsilon_{cm}(N)}{dN} \right)_{N=0}, \tag{27}$$

where A'_0, B'_0 , and C'_0 are the initial values of $A', B',$ and C' , respectively.

By substituting Equation (27) into Equation (25) and eliminating $\left(\frac{d\xi_n}{dN} \right)_0$, the equation is derived as

$$\begin{aligned}
 a &= D_0 \cdot (A_0 + B_0 + C_0)^P \cdot \\
 &\left\{ \frac{6H^2 \xi_0^4 (A_0 + B_0 + C_0)^2}{-H_0^2 \varepsilon_m(0) \cdot [2\xi_0 \cdot (A_0 + B_0 + C_0) + \xi_0^2 \cdot (A'_0 + B'_0 + C'_0)]} \cdot \left(\frac{d\varepsilon_m(N)}{dN} \right)_{N=0} \right\}. \tag{28}
 \end{aligned}$$

When fatigue cracks initiate, the parameter $D_{cm}(N)$ is equal to 1.0. By substituting Equation (28) into Equation (24), the formula for predicting the fatigue life N_f of steel deck FRAC surfacing can deduced as

$$N_f = \left\{ \frac{-H_0^2 \cdot [2\xi_0 \cdot (A_0 + B_0 + C_0) + \xi_0^2 \cdot (A'_0 + B'_0 + C'_0)]}{6H^2 \xi_0^4 (A_0 + B_0 + C_0)^2} \cdot \int_{\xi_0}^{\xi_n} D \cdot (A + B + C)^P d\xi_n \right\} \cdot \left\{ \varepsilon_{cm}(0) / \left(\frac{d\varepsilon_{cm}(N)}{dN} \right)_{N=0} \right\}. \tag{29}$$

It is assumed that the fatigue life of the FRAC surfacing can be derived by setting parameter P equal to 1, that is, the fatigue damage evolution process is a linear relationship. Then, the fatigue life of the surfacing layer can be obtained by substituting $p = 1$ into Equation (29). After N loading cycles, the fatigue crack forms and damage reaches a peak, i.e., $D_{cm}(N)$ is equal to 1.0. The neutral axis position ξ_n can be obtained by substituting into Equation (12).

4. Fatigue Experiment

4.1. Raw Material Design and Road Performance Test of Gussasphalt (GA) mixture

The Gussasphalt mixture refers to a kind of asphalt mixture with high asphalt content, high mineral powder content, and a void ratio less than 1%, which is mixed at high temperature (220–260 °C), spread and formed by its own fluidity, and does not need to be rolled. Gussasphalt is usually composed of Lake Asphalt and petroleum asphalt in a certain proportion. Mixture design is one of the key technologies for comprehensively balancing the material performance. Reasonable design methods and design parameters are the key to achieving this comprehensive balance. Basalt is used as the aggregate in the GA mixture, and the percentage share of all components of the GA mix is presented in Table 1.

Table 1. Percentage shares of all components for the Gussasphalt (GA) mixture.

Component	Percentage (%)
Coarse aggregate	47.0
Fine aggregate	27.3
Mineral powder	19.6
Asphalt	6.1

Note: The coarse aggregate size is greater than 2.36 mm; the fine aggregate size is less than 2.36 mm and greater than 0.075 mm.

The main performance indexes of the asphalt mixture are its indirect tensile strength, rut resistance, Marshall stability, and immersion Marshall stability. According to the corresponding test standards, each of these GA mixture performance indexes is shown in Table 2.

Table 2. Technical performances and specifications for the GA mixture.

Performance	Test Result	Test Method	Specifications
Dynamic stability (mm)	1.02	T0719-2011 [42]	-
60 °C cured Marshall stability (kN)	26.5	ASTM D6927 [43]	≥40
Immersion Marshall stability (%)	90.7	ASTM D6927 [43]	≥85
Indirect tensile strength (MPa)	2.39	T0716-2011 [42]	-

The test results in Table 2 show that the rutting deformation of GA is only 1.02 mm in 60 min, which indicates that the GA used in this study has good thermal stability. The Marshall stability increases with the increasing curing time, but the Marshall stability of the uncured specimen is lower than that of the cured ones, which implies that reasonable curing can increase the Marshall stability of the GA mixture. The residual stability of GA sample after soaking is more than 85%, which means that the soaking time does not significantly influence the residual stability, and the water stability performance of GA mixture is good. The trend in the indirect tensile strength is similar to that of the Marshall stability for the GA mixture.

4.2. Raw Materials Design and Performance Test of Polyacrylonitrile (PAN) Fiber

In order to study the effect of R_a and V_f on the fatigue properties of GA, the characteristic geometric parameters of PAN fiber are shown in Table 3.

Table 3. Characteristic geometric parameters of polyacrylonitrile (PAN) fiber.

Parameter	Average Length (mm)	Average Diameter (μm)	Volume Ratio (%)
1	3	12.5	0.1
2	6		0.3
3	9		0.5
4	12		0.7

The PAN fiber shown in Figure 2 was used as the raw material, and its technical indexes were tested, as shown in Table 4.



Figure 2. PAN fiber for the test.

Table 4. Characteristics of the PAN fiber.

Performance	Tensile Strength	Elastic Modulus	Elongation	Density	Titer	Melting Point	Dispersion
Test Condition, Unit	Dry, MPa	GPa	%	g/cm ³	dtex	°C	-
Specifications	>1640	>38.1	5–9	1.29–1.30	1.7–2.3	255–260	1–3
Test Result	1725.28	39.71	6.47	1.291	2.01	259	1

4.3. Fatigue Measurement of the Composite Beam for the Steel Deck FRAC Surfacing

The environmental temperature and the cycling vehicle load are important factors that affect the tensile stress/strain and fatigue resistance of the steel bridge surface. In order to simulate the actual stress state of steel deck surfacing, the vehicle load was applied on the top of a U-shaped stiffener. Thus, the steel plate was pasted on top of the FRAC beam to form the composite beam, which could bear the cycling load. The most unfavorable condition for fatigue cracking of bridge deck surfacing occurs in medium- and low-temperature environments [44,45]. In order to study the effect of temperature, these tests were carried out at 60, 20, and -15 °C. During the fatigue test on the composite beam, the length of the fiber in the FRAC surfacing was set to 3, 6, 9, and 12 mm, and the volume ratio of fiber was set to 0.1%, 0.3%, 0.5%, and 0.7% (see Table 4).

According to the structural characteristics of Jiangyin Yangtze River Bridge, the composite beams for the fatigue test were designed based on the models. Under the action of standard axle load (BZZ-100), the cyclic load amplitude was 5 kN [46]. Generally, the traveling speed of vehicles on the steel bridge surface is between 50 km/h and 100 km/h, and the corresponding fatigue loading frequency is 5–10 Hz. The results of fatigue test of composite beams show that the change in the loading frequency between 5 Hz and 10 Hz negligibly affects the fatigue behavior. Therefore, the fatigue loading frequency of this experiment was 10 Hz, and the loading form was sinusoidal.

5. Results and Discussions

5.1. Influence of Fiber Length on Fatigue Performance of Steel Deck AC Surfacing

The relationships between the bottom edge strain of middle span on the composite beam $\varepsilon_{cm}(N)$ and the number of fatigue load cycles N with a PAN fiber volume ratio of 0.4%, fiber lengths of 3, 6, 9, and 12 mm, and ambient temperatures of -15 , 20, and 60 °C are presented in Figure 3a–c, respectively. The results were fitted using Equation (19), as shown by the dotted lines in Figure 3. This figure shows that the fitting results are in good agreement with the experimental results, indicating that Equation (19) effectively describes the relationship between bottom edge strain $\varepsilon_{cm}(N)$ and fatigue load cycles N .

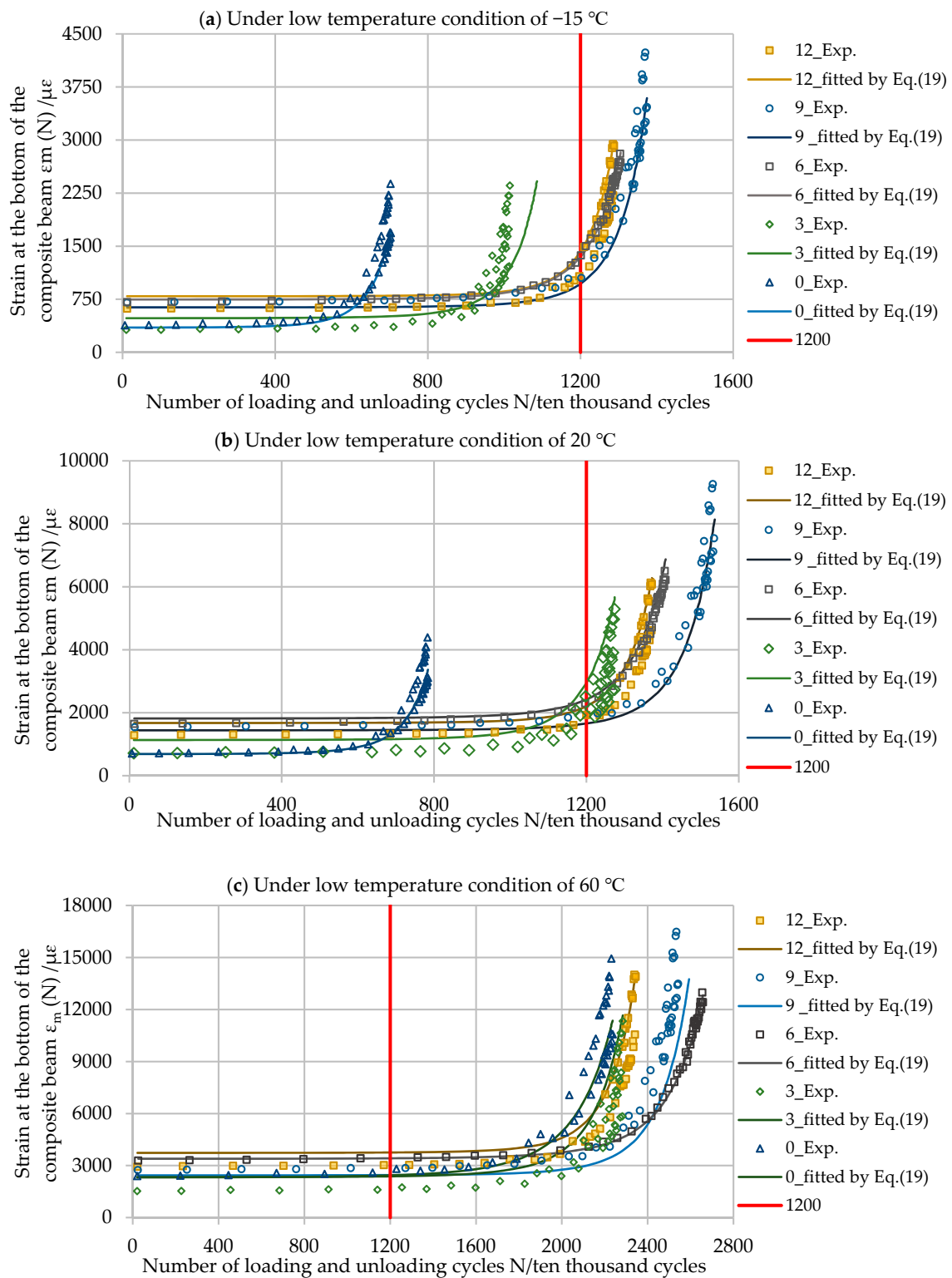


Figure 3. The relationships between the bottom edge strain $\epsilon_{cm}(N)$ and fatigue load cycles N under different ambient temperatures and with fiber lengths of 3, 6, 9, and 12 mm: (a) under ambient temperature conditions, $60\text{ }^\circ\text{C}$; (b) under normal temperature conditions, $20\text{ }^\circ\text{C}$; (c) under ambient temperature conditions, $-15\text{ }^\circ\text{C}$. Note: The red line denotes “1200/10,000 cycles,” which is the design standard for steel deck AC surfacing [47].

The results of Figure 3 show that the strain $\epsilon_m(N)$ at the bottom of the composite beam for the steel deck FRAC surfacing increases with increasing temperature, and the deformation resistance and

fatigue resistance are significantly improved. The reason for this improvement is that the asphalt mixture has a certain creep performance at high temperature. The repeated tensile and compressive strain is conducive to the rapid recovery of material deformation and effectively shortens the tensile stress time of the GA-PAN mixture. At the same time, the elastic modulus of GA-PAN concrete decreases at high temperature, which obviously decreases the material fatigue stress and then increases the fatigue resistance of the GA-PAN surfacing. Therefore, the fatigue failure of steel bridge asphalt surfacing usually occurs at normal temperature (20 °C) and during low-temperature seasons (−15 °C). According to the findings of this study, the anti-deformation and anti-cracking performance of AC surfacing can be effectively improved by using a certain fiber length under normal temperature (20 °C) and low-temperature conditions (−15 °C). Theoretically, a greater fiber length results in a higher fatigue resistance of GA-PAN surfacing. However, when the fiber length exceeds 9 mm, the synergistic effect, which is related to mixing uniformity, is relatively less obvious because a longer fiber renders it more difficult to mix.

According to the fatigue test results, the fitting results of the relationship between the initial strain $\varepsilon_{cm}(0)$ and the initial strain rate $(d\varepsilon_{cm}(N)/dN)_0$ at the bottom of the composite beam are shown in Figure 3. By substituting the data of $\varepsilon_{cm}(0)$ and $(d\varepsilon_{cm}(N)/dN)_0$ into Equation (29), the fatigue life for steel deck GA-PAN surfacing under different temperature conditions and fiber lengths can be predicted.

The theoretically predicted value and test results of the fatigue life of steel bridge deck GA-PAN surfacing are compared in Figure 4, which shows that they are in good agreement, and the error is within 10%. These findings verify the rationality and scientific relevance of the theoretical model. It is worth noting that the theoretically predicted value is generally slightly higher than the experimental results. Temperature is one of the main factors that affect the fatigue life of the steel bridge deck GA-PAN surfacing. Figure 4b shows that, with the decreasing temperature, the synergism of fiber is more pronounced. Therefore, under the sensitive conditions for fatigue failure, i.e., low temperature, steel bridge GA-PAN surfacing mixed with fiber of a certain length can effectively alleviate the fatigue crack in asphalt pavement. The best fiber length is 9 mm, which meets the design requirements of the steel deck surfacing ($N_f > 1200/10,000$ cycles) at low temperature (−15 °C) and normal temperature (20 °C) [47].

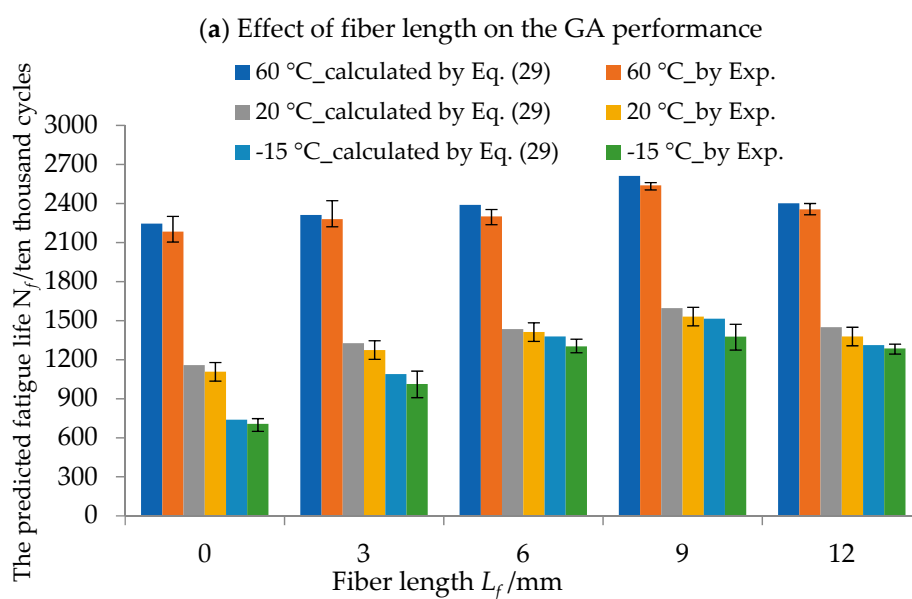


Figure 4. Cont.

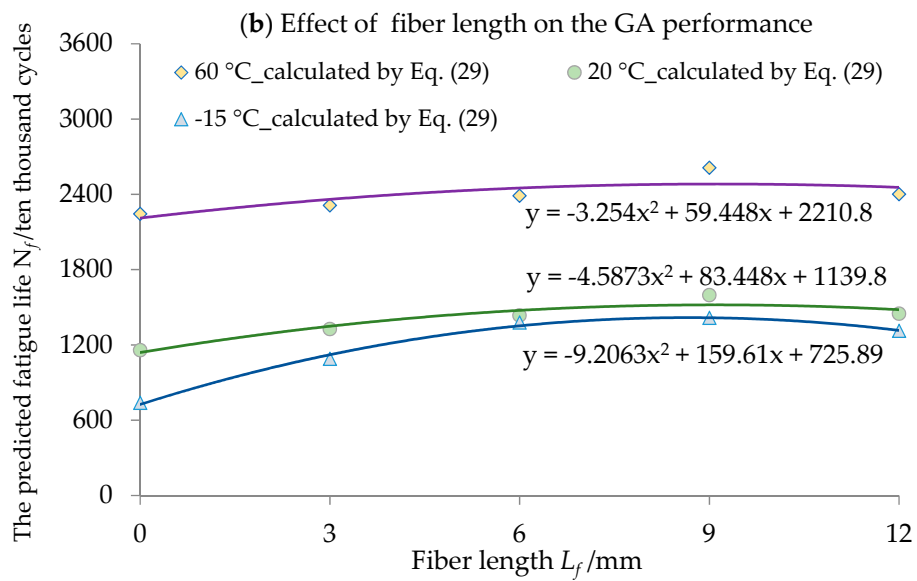


Figure 4. Comparison between predicted and measured fatigue life for different temperatures and fiber lengths (tested under standard axle load, BZZ-100) (unit: 10,000 cycles). (a) Effect of fiber length on the GA performance (the theoretically predicted value and test results); (b) Effect of fiber length on the GA performance.

5.2. Influence of Fiber Content on Fatigue Performance of Steel Deck AC Surfacing

The relationships between the bottom edge strain of the middle span on the composite beam $\epsilon_{cm}(N)$ and the number of fatigue load cycles N with a PAN fiber length of 9 mm, volume ratio of 0%, 0.1%, 0.3%, 0.5%, and 0.7%, and ambient temperatures of -15 , 20, and 60 °C are presented in Figure 5a–c, respectively. The results fitted with Equation (19) are also shown as dotted lines this figure, which shows that the fitting results are in good agreement with the experimental results. Therefore, Equation (19) can effectively describe the relationship between the bottom edge strain $\epsilon_{cm}(N)$ and the fatigue load cycles N .

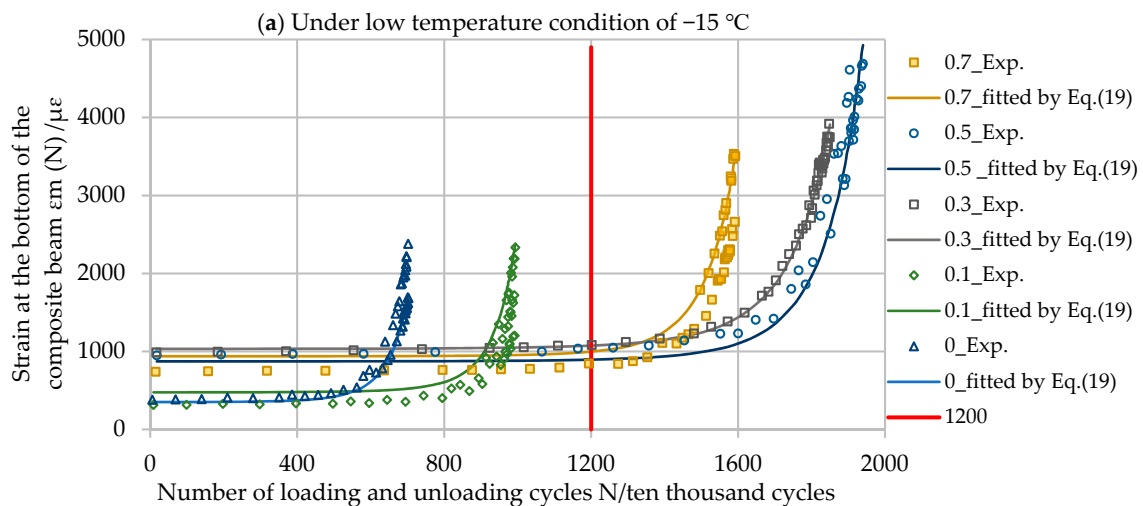


Figure 5. Cont.

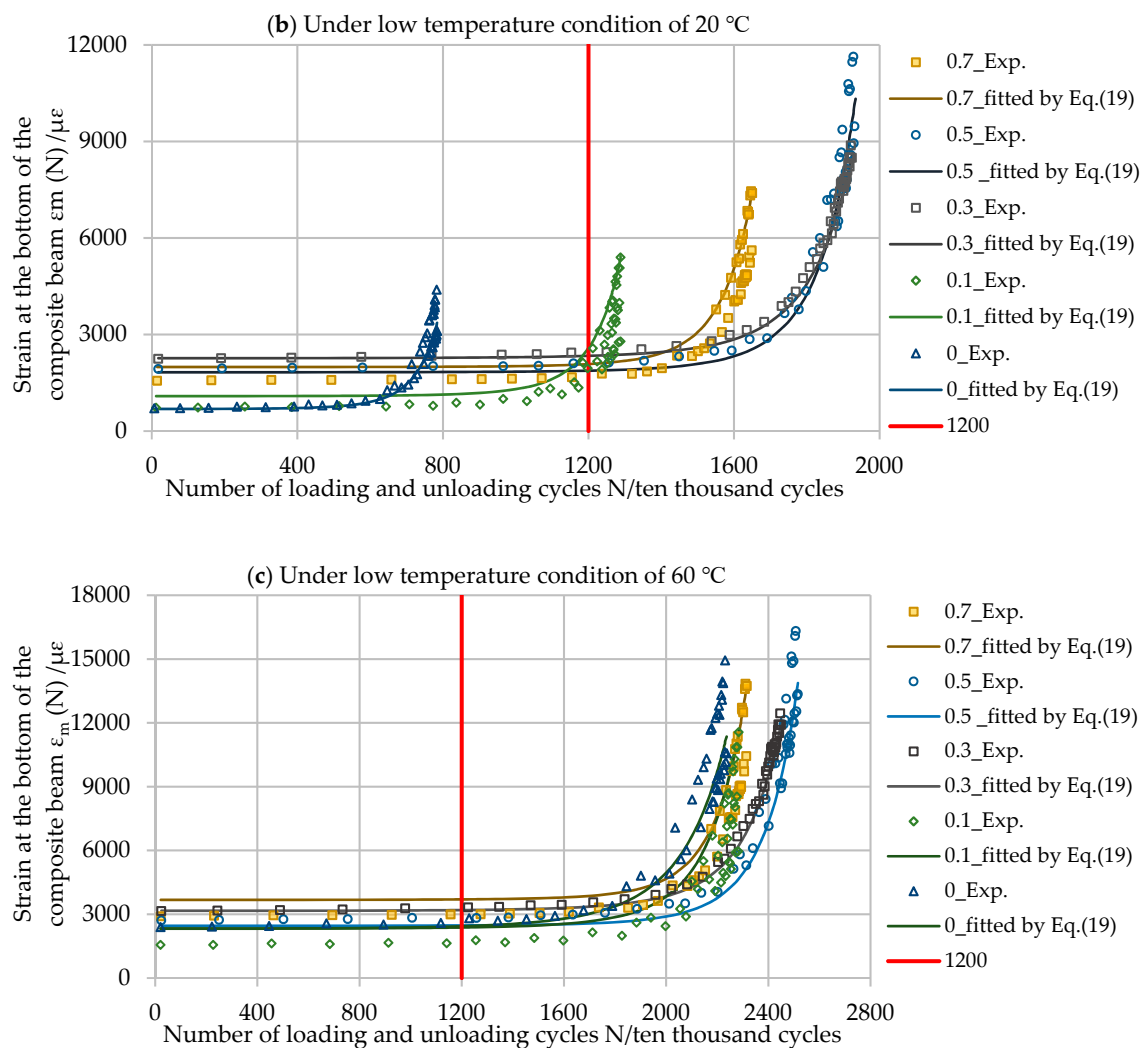


Figure 5. Relationships between the bottom edge strain $\epsilon_{cm}(N)$ and fatigue load cycles N under different ambient temperatures and with fiber volume ratios of 0%, 0.1%, 0.3%, 0.5%, and 0.7%: (a) under high-temperature conditions, 60 °C; (b) under normal temperature condition, 20 °C; (c) under low-temperature conditions, −15 °C. Note: The red line represents “1200/10,000 cycles,” which is the design standard for steel deck AC surfacing [47].

The results of Figure 5 show that adding a certain proportion of PAN fiber can effectively increase the deformation and crack resistance of asphalt surfacing at normal (20 °C) and low temperature (−15 °C). Theoretically, greater fiber integration results in higher fatigue resistance of the asphalt surface. However, when the fiber volume ratio is more than 0.5%, the synergistic effect, which is not related to mixing uniformity, is not pronounced because longer fibers are more difficult to mix.

According to the fatigue test results, the fitting results of the relationship between the initial strain $\epsilon_{cm}(0)$ and the initial strain rate $(d\epsilon_{cm}(N)/dN)_0$ at the bottom of the composite beam are shown in Figure 5. By substituting the data of $\epsilon_{cm}(0)$ and $(d\epsilon_{cm}(N)/dN)_0$ into Equation (29), the fatigue life for steel deck GA-PAN surfacing under different temperature conditions and with different fiber contents can be predicted.

The calculation process is the same as that used in Section 5.1. Substituting the data of $\epsilon_{cm}(0)$ and $(d\epsilon_{cm}(N)/dN)_0$ (shown in Figure 5) into Equation (29), the fatigue life of steel deck GA-PAN surfacing under different temperature conditions and fiber volume ratios can be calculated. The theoretically predicted value and experimentally tested fatigue life values of steel bridge deck FRAC surfacing, which are compared in Figure 6, are in good agreement, and the error is within 12%. Figure 6 shows

that, with the decreasing temperature, the synergistic effect of the fiber is more significant. Therefore, under the sensitive conditions for fatigue failure, i.e., low temperature, steel bridge GA-PAN surfacing mixed with fiber with a certain content ration can effectively alleviate the fatigue cracking of asphalt pavement. The best fiber volume ratio is 0.46%–0.48%, which meets the design requirements for the steel deck surfacing ($N_f > 1200/10,000$ cycles) at low temperature (−15 °C) and normal temperature (20 °C) [47].

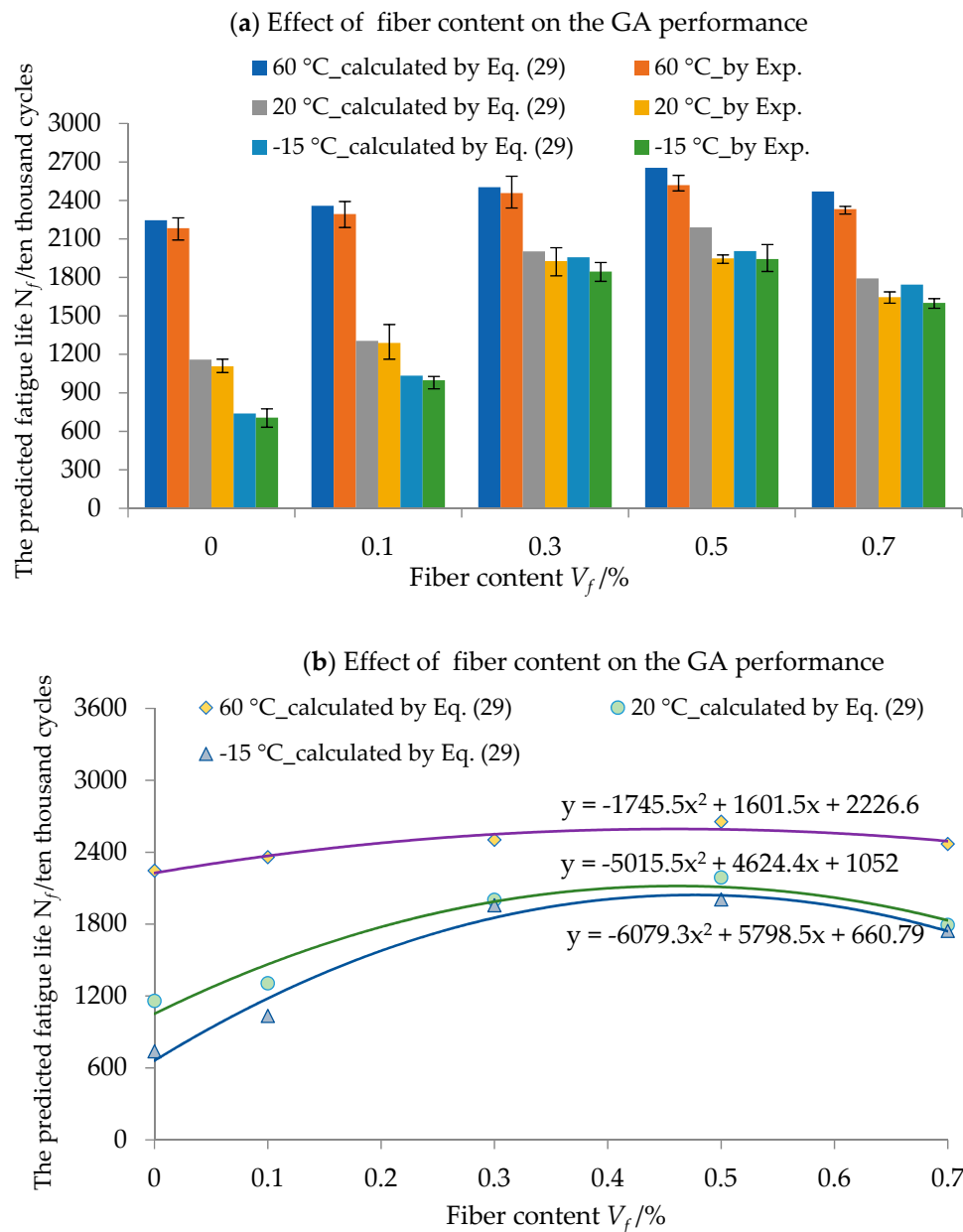


Figure 6. Comparison between the predicted and measured fatigue life under different temperatures and fiber contents (tested under standard axle load, BZZ-100) (unit: 10,000 cycles). (a) Effect of fiber length on the GA performance (the theoretically predicted value and test results); (b) Effect of fiber length on the GA performance.

6. Conclusions

Based on the continuous damage mechanics method, a model for crack initiation and the fatigue life predicting of FRAC surfacing for steel bridge decks was established, and the feasibility of the model was verified via GA-PAN surfacing fatigue tests. The results are outlined below.

Temperature is the main factor affecting the fatigue performance of AC surfacing on the steel bridge deck. With decreasing temperature, the elastic modulus of AC surfacing increases, which increases the peak stress in the sensitive area and reduces the fatigue resistance of the surfacing. FRAC has higher strength, deformation resistance, and fatigue resistance than AC concrete at different temperatures. Therefore, using FRAC surfacing as a bridge deck surfacing material can significantly improve the fatigue performance of bridge deck AC surfacing.

The length L_f and the ratio of fiber volume V_f significantly influence the fatigue life of the steel bridge deck FRAC surfacing. With increasing fiber length and fiber volume ratio, the fatigue life of bridge deck FRAC surfacing gradually increases. In the case of the GA-PAN surfacing, the optimal fiber length and mixing ratio are 9 mm and 0.46%–0.48%, respectively, which provide good fatigue resistance and meet the design requirements of steel bridge deck surfacing at low temperature ($-15\text{ }^\circ\text{C}$) [47].

The model can provide predictions for the crack initiation and fatigue life of steel bridge deck FRAC surfacing. However, note that this study does not consider the influence of temperature field unevenness, initial defects (voids, microcracks), interface characteristics between fiber and AC, or fiber material type and geometry on the fatigue life of steel bridge deck AC surfacing. In order to further increase the accuracy of the fatigue life model, the above factors should be considered in the prediction model of the steel bridge deck FRAC surfacing. Thus, road performances of steel bridge deck AC surfacing under various fiber material types, geometric characteristics, and interface characteristics should be studied, which will be the subject of future work.

Author Contributions: Conceptualization, X.Q.X. and H.L.X.; methodology, H.L.X.; software, W.Y.; formal analysis, X.Q.X.; investigation, X.Y.; visualization, J.B.W.; supervision, X.Q.X. All authors have read and agreed to the published version of the manuscript.

Funding: This research was funded by the National Natural Science Foundation of China, No. 2016YFB0303100, the Natural Science Foundation of Jiangsu Province, No. BK20171254, the Jiangsu University Student Innovation Training Program, No. 201910304100Y, the Natural Science Foundation of Nantong, No. JC2018095 and JC2019065.

Conflicts of Interest: The authors declare no conflict of interest.

References

1. Wolchuk, R. Orthotrope Fahrbahnplatte—Entwicklungen und Möglichkeiten für die Zukunft. *Stahlbau* **2007**, *76*, 478–494. [[CrossRef](#)]
2. Hornyak, N.; Crovetto, J.A. Analysis of load pulse durations for Marquette interchange instrumentation project. *Transp. Res. Rec.* **2009**, *2094*, 53–61. [[CrossRef](#)]
3. Medani, T.O.; Liu, X.; Huurman, M.; Scarpas, A.; Molenaar, A.A.A. Characterisation of surfacing materials for orthotropic steel deck bridges. Part 1: Experimental work. *Int. J. Surf. Eng.* **2010**, *11*, 237–253. [[CrossRef](#)]
4. Kozy, B.M.; Connor, R.J.; Paterson, D.; Mertz, D.R. Proposed revisions to AASHTO-LRFD bridge design specifications for orthotropic steel deck bridges. *J. Bridge Eng.* **2010**, *16*, 759–767. [[CrossRef](#)]
5. Bayat, A.; Knight, M. Field evaluation and analysis of flexible surfacing structural responses under dynamic loads. *Road Mater. Surf. Des.* **2012**, *13*, 26–37.
6. Ameri, M.; Nowbakht, S.; Molayem, M.; Mirabimoghaddam, M.H. A study on fatigue modeling of hot mix asphalt mixtures based on the viscoelastic continuum damage properties of asphalt binder. *Constr. Build. Mater.* **2016**, *106*, 243–252. [[CrossRef](#)]
7. Santagata, E.; Baglieri, O.; Dalmazzo, D.; Tsantilis, L. Investigating cohesive healing of asphalt binders by means of a dissipated energy approach. *Int. J. Surf. Res. Technol.* **2017**, *10*, 403–409. [[CrossRef](#)]
8. Huang, W. Integrated Design Procedure for Epoxy Asphalt Concrete–Based Wearing Surface on Long-Span Orthotropic Steel Deck Bridges. *J. Mater. Civ. Eng.* **2015**, *28*, 04015189. [[CrossRef](#)]
9. Chavel, B. *Steel Bridge Design Handbook: BRIDGE Deck Design, Rep. No. FHWA-IF-12-052-Volume 17*; Federal Highway Administration: Washington, DC, USA, 2012.
10. Kainuma, S.; Jeong, Y.S.; Ahn, J.-H.; Yamagami, T.; Tsukamoto, S. Behavior and stress of orthotropic deck with bulb rib by surface corrosion. *J. Constr. Steel Res.* **2015**, *113*, 135–145. [[CrossRef](#)]
11. Chenjs, L.K.Y. Mechanism and behavior of bitumen strength reinforcement using fibers. *J. Mater. Sci.* **2005**, *40*, 87–95.

12. Putman, B.J.; Amirkhani, S.N. Utilization of waste fibers in stone matrix asphalt mixtures. *J. Resour. Conserv. Recyc.* **2004**, *42*, 265–274. [[CrossRef](#)]
13. Barra, B.; Momm, L.; Guerrero, Y.; Bernucci, L. Fatigue behavior of dense asphalt mixes in dry and environmental-conditioning states. *J. Constr. Build. Mat.* **2012**, *29*, 128–134. [[CrossRef](#)]
14. Erdem, C.; John, T.H.; Yang, K.; Boone, J.M. A micromechanical approach to investigate asphalt concrete rutting mechanisms. *J. Constr. Build. Mat.* **2012**, *30*, 36–49.
15. Adhikari, S.; You, Z.; Hao, P.W.; Wang, H.N. Image Analysis of aggregate, mastic and air void phases for asphalt mixture. *J. Traffic Transp.* **2013**, *13*, 1–9.
16. Ebrahim, S.; Hasan, Z.; Maryam, S. The effect of aggregate gradation limits consideration on performance properties and mixture design parameters of hot mix asphalt. *J. Civ. Eng.* **2016**, *20*, 385–392.
17. Liu, Q.; Schlangen, E.; van de Ven, M.; van Bochove, G.; van Montfort, J. Evaluation of the induction healing effect of porous asphalt concrete through four point bending fatigue test. *Constr. Build. Mat.* **2012**, *29*, 403–409. [[CrossRef](#)]
18. Yin, C.; Zhang, H.; Pan, Y. Cracking mechanism and repair techniques of epoxy asphalt on steel bridge deck surfacing. *Transp. Res. Rec.* **2016**, *2550*, 123–130. [[CrossRef](#)]
19. Kainuma, S.; Yang, M.; Jeong, Y.S.; Inokuchi, S.; Kawabata, A.; Uchida, D. Experimental investigation for structural parameter effects on fatigue behavior of rib-to-deck welded joints in orthotropic steel decks. *Eng. Fail. Anal.* **2017**, *79*, 520–537. [[CrossRef](#)]
20. Zhong, K.; Yang, X.; Wei, X. Investigation on surface characteristics of epoxy asphalt concrete surfacing. *Int. J. Surf. Res. Technol.* **2017**, *10*, 545–552.
21. Wang, Z.; Zhang, S. Fatigue endurance limit of epoxy asphalt concrete surfacing on the deck of long-span steel bridge. *Int. J. Surf. Res. Technol.* **2018**, *11*, 408–415.
22. Zhang, L.; Wang, W.; Lu, Q.; Chen, X. An innovative approach to determine deck surfacing modulus and interfacial slip stiffness based on a composite beam model. *Constr. Build. Mater.* **2013**, *40*, 411–418. [[CrossRef](#)]
23. Bocci, E.; Graziani, A.; Canestrari, F. Mechanical 3D characterization of epoxy asphalt concrete for surfacing layers of orthotropic steel decks. *Constr. Build. Mater.* **2015**, *79*, 145–152. [[CrossRef](#)]
24. Harvey, J.T.; Deacon, J.A.; Tsai, B.W.; Monismith, C.L. *Fatigue Performance of Asphalt Concrete Mixes and Its Relationship to Asphalt Concrete Surfacing Performance in California*; University of California: Cambridge, MA, USA, 1995.
25. Sousa, J.B.; Pais, J.C.; Prates, M.; Barros, R.; Langlois, P.; Leclerc, A.M. Effect of aggregate gradation on fatigue life of asphalt concrete mixes. *Transp. Res. Rec.* **1998**, *1630*, 62–68. [[CrossRef](#)]
26. Yoo, P.J.; Al-Qadi, I.L. A strain-controlled hot-mix asphalt fatigue model considering low and high cycles. *Int. J. Surf. Eng.* **2010**, *11*, 565–574. [[CrossRef](#)]
27. Pokorski, P.; Radziszewski, P.; Sarnowski, M. Fatigue life of asphalt surfacings on bridge decks. *Procedia Eng.* **2016**, *153*, 556–562. [[CrossRef](#)]
28. Alencar, G.; de Jesus, A.M.P.; Calçada, R.A.B.; da Silva, J.G.S. Fatigue life evaluation of a composite steel-concrete roadway bridge through the hot-spot stress method considering progressive surfacing deterioration. *Eng. Struct.* **2018**, *166*, 46–61. [[CrossRef](#)]
29. Qian, Z.D.; Wang, J.Y.; Chen, L.L.; Wang, L.B. Three-dimensional discrete element modeling of crack development in epoxy asphalt concrete. *J. Test. Eval.* **2014**, *43*, 1–13. [[CrossRef](#)]
30. Garcia, G.; Thompson, M.R. Strain and pulse duration considerations for extended-life hot-mix asphalt surfacing design. *Transp. Res. Rec.* **2008**, *2087*, 3–11. [[CrossRef](#)]
31. Campbell, F.C. *Fatigue and Fracture: Understanding the Basics*; ASM International: Materials Park, OH, USA, 2012.
32. Shen, S.; Chiu, H.M.; Huang, H. Characterization of fatigue and healing in asphalt binders. *J. Mater. Civil Eng.* **2010**, *22*, 846–852. [[CrossRef](#)]
33. Saboo, N.; Kumar, P. Optimum blending requirements for EVA modified binder. *Int. J. Surf. Res. Technol.* **2015**, *8*, 172–178. [[CrossRef](#)]
34. Delgadillo, R.; Bahia, H.U.; Lakes, R. A nonlinear constitutive relationship for asphalt binders. *Mater. Struct.* **2012**, *45*, 457–473. [[CrossRef](#)]
35. Zhang, X.C.; Huang, W.; Wei, Q.; Zhang, J.; Tong, X.D. A fatigue damage analysis of composite construction composed asphalt concrete surfacing and steel-box beam deck of steel bridge. *Key Eng. Trans. Tech. Pub.* **2004**, *274*, 223–228.

36. Liu, W.; Xu, S.; Li, Q. Experimental study on fracture performance of ultra-high toughness cementitious composites with J-integral. *Eng. Fract. Mech.* **2012**, *96*, 656–666. [[CrossRef](#)]
37. Teixeira de Freitas, S.; Kolstein, H.; Bijlaard, F. Fatigue assessment of full-scale retrofitted orthotropic bridge decks. *J. Bridge Eng.* **2017**, *22*, 04017092. [[CrossRef](#)]
38. Brovelli, C.; Crispino, M.; Pais, J.; Pereira, P.A. Assessment of fatigue resistance of additivated asphalt concrete incorporating fibers and polymers. *J. Mater. Civ. Eng.* **2014**, *26*, 554–558. [[CrossRef](#)]
39. Lee, S.J.; Rust, J.P.; Hamouda, H.; Kim, Y.R.; Borden, R.H. Fatigue cracking resistance of fiber reinforced asphalt concrete. *Text. Res. J.* **2005**, *75*, 123–128. [[CrossRef](#)]
40. Losa, M.; Di Natale, A. Evaluation of representative loading frequency for linear elastic analysis of asphalt surfacing. *Transp. Res. Rec.* **2012**, *2305*, 150–161. [[CrossRef](#)]
41. Kachanov, K. Elastic solids with many cracks and related problems. *Adv. Appl. Mech.* **1993**, *30*, 259–445.
42. JTG E20-2011. *Standard Test Material of Bitumen and Bituminous Mixtures for Highway Engineering*, CN-JT; China Communications Press: Beijing, China, 2011.
43. ASTM D6927. *Standard Test Method for Marshall Stability and Flow of Asphalt Mixtures*; ASTM International: West Conshohocken, PA, USA, 2015.
44. Kim, T.W.; Baek, J.; Lee, H.J.; Lee, S.Y. Effect of surfacing design parameters on the behavior of orthotropic steel bridge deck surfacings under traffic loading. *Int. J. Surf. Eng.* **2014**, *15*, 471–482.
45. Cheng, H.; Liu, L.; Sun, L. Field measurements of dynamic strain responses of asphalt surfacing on steel deck bridge. *China Civ. Eng. J.* **2019**, *52*, 100–108.
46. Xu, X.; Yang, X.; Huang, W.; Xiang, H.; Yang, W. New damage evolution law for steel–asphalt concrete composite pavement considering wheel load and temperature variation. *Materials* **2019**, *12*, 3723. [[CrossRef](#)] [[PubMed](#)]
47. JTG D50-2017. *Specifications for Design of Highway Asphalt Surfacing*, CN-JT; China Communications Press: Beijing, China, 2017.



© 2020 by the authors. Licensee MDPI, Basel, Switzerland. This article is an open access article distributed under the terms and conditions of the Creative Commons Attribution (CC BY) license (<http://creativecommons.org/licenses/by/4.0/>).